AFRL-RY-WP-TR-2015-0071

APPLICATION OF COMPRESSIVE SENSING TO DIGITAL HOLOGRAPHY

Mark Neifeld
University of Arizona

MAY 2015
Final Report

AIR FORCE RESEARCH LABORATORY
SENSORS DIRECTORATE
WRIGHT-PATTERSON AIR FORCE BASE, OH 45433-7320
AIR FORCE MATERIEL COMMAND
UNITED STATES AIR FORCE

NOTICE AND SIGNATURE PAGE

Using Government drawings, specifications, or other data included in this document for any purpose other than Government procurement does not in any way obligate the U.S. Government. The fact that the Government formulated or supplied the drawings, specifications, or other data does not license the holder or any other person or corporation; or convey any rights or permission to manufacture, use, or sell any patented invention that may relate to them.

This report was cleared for public release by the USAF 88th Air Base Wing (88 ABW) Public Affairs Office (PAO) and is available to the general public, including foreign nationals. Copies may be obtained from the Defense Technical Information Center (DTIC) (http://www.dtic.mil).

AFRL-RY-WP-TR-2015-0071 HAS BEEN REVIEWED AND IS APPROVED FOR PUBLICATION IN ACCORDANCE WITH ASSIGNED DISTRIBUTION STATEMENT.

// Signature//

DAVID J. RABB
Program Manager
LADAR Technology Branch
Multispectral Sensing and Detection Division

// Signature//

BRIAN D. EWERT, Chief
LADAR Technology Branch
Multispectral Sensing and Detection Division

// Signature//

TRACY W. JOHNSTON, Chief
Multispectral Sensing and Detection Division
Sensors Directorate

This report is published in the interest of scientific and technical information exchange, and its publication does not constitute the Government's approval or disapproval of its ideas or findings.

*Disseminated copies will show "//Signature//" stamped or typed above the signature blocks.

REPORT DOCUMENTATION PAGE

Form Approved
OMB No. 0704-0188

1. REPORT DATE *(DD-MM-YY)*	2. REPORT TYPE	3. DATES COVERED *(From - To)*
May 2015	Final	3 September 2013 – 27 February 2015

4. TITLE AND SUBTITLE
APPLICATION OF COMPRESSIVE SENSING TO DIGITAL HOLOGRAPHY

5a. CONTRACT NUMBER
FA8650-13-1-7374

5b. GRANT NUMBER

5c. PROGRAM ELEMENT NUMBER
63767E

6. AUTHOR(S)
Mark Neifeld

5d. PROJECT NUMBER
3000

5e. TASK NUMBER
N/A

5f. WORK UNIT NUMBER
Y12Y

7. PERFORMING ORGANIZATION NAME(S) AND ADDRESS(ES)

University of Arizona
888 N. Euclid Avenue
Tucson, AZ 85719-4824

8. PERFORMING ORGANIZATION REPORT NUMBER

9. SPONSORING/MONITORING AGENCY NAME(S) AND ADDRESS(ES)

Air Force Research Laboratory
Sensors Directorate
Wright-Patterson Air Force Base, OH 45433-7320
Air Force Materiel Command
United States Air Force

10. SPONSORING/MONITORING AGENCY ACRONYM(S)
AFRL/RYMM

11. SPONSORING/MONITORING AGENCY REPORT NUMBER(S)
AFRL-RY-WP-TR-2015-0071

12. DISTRIBUTION/AVAILABILITY STATEMENT
Approved for public release; distribution unlimited.

13. SUPPLEMENTARY NOTES
The U.S. Government is joint author of the work and has the right to use, modify, reproduce, release, perform, display or disclose the work. PAO case number 88ABW-2015-2052, Clearance Date 22 April 2015. Report contains color.

14. ABSTRACT
Compressive sensing has been used in many imaging domains to facilitate high quality reconstruction from under-sampled data. This work presents a new reconstruction algorithm for use with under-sampled digital holography measurements and yields reconstruction quality far superior to conventional backpropagation methods. The report describes the new dictionary prior and its use in an iterative soft thresholding algorithm and presents systematic studies of performance versus various physical variables such as exposure time, degree of under-sampling, and object sparsity.

15. SUBJECT TERMS
digital holography, compressive sensing

16. SECURITY CLASSIFICATION OF:			17. LIMITATION OF ABSTRACT:	18. NUMBER OF PAGES	19a. NAME OF RESPONSIBLE PERSON (Monitor)
a. REPORT	b. ABSTRACT	c. THIS PAGE			David Rabb
Unclassified	Unclassified	Unclassified	SAR	20	19b. TELEPHONE NUMBER *(Include Area Code)* N/A

Table of Contents

Section **Page**

List of Figures

Figure **Page**

Acknowledgements

This work was supported by the Air Force Research Laboratory (AFRL) and the Defense Advanced Research Agency (DARPA) under agreement number FA8650-13-1-7374.

1.0 SUMMARY

Sparse aperture (SA) digital holography (DH) is a potentially valuable tool for 3D imaging within many commercial and military applications. By employing a common reference field across sub-apertures, this form of DH enables coherent phase measurements to be obtained over the full optical aperture leading to excellent 3D resolution in a compact low-cost package. However, the image quality obtained from such a system is seen to degrade quickly as SA fill-factor is reduced. The two primary reasons for this degradation are (a) missing data and/or aliasing associated with under-sampling and (b) SNR reduction associated with fewer collected photons. Our work in this project has demonstrated that compressive sensing (CS) techniques may be employed to improve reconstructed image quality. We demonstrate DH reconstructions that exploit a sparse dictionary prior and we quantitatively compare the performance of CS and non-CS based methods as a functions of measurement SNR, aperture sparsity, and degree of focal plane under-sampling.

2.0 INTRODUCTION

Sampling of continuous signals in space/time/wavelength has become ubiquitous in modern digital imaging and other sensing systems. The Nyquist theorem (1,2) forms the mathematical foundation of the relevant sampling theory and it specifies that a band-limited signal can be sampled at the Nyquist rate (i.e., twice the highest frequency) without any loss of information. However, most signals of interest possess additional structure that can reduce the inherent degrees of freedom required to uniquely describe the signal. For example, natural scenes tend to be spatially correlated and therefore sparse or compressible in some transform domain. Such signals can be sampled at sub-Nyquist rates with minimal or sometimes no loss of information. This fact forms the basis of the many widely successful post-measurement image compression algorithms such as JPEG2000 which regularly yield compression ratios of 10x or greater without loss of visual quality.(3) The CS theory rigorously proves that under certain conditions, sub-Nyquist sampling can be sufficient to reconstruct a sparse signal with no loss of information.(4-7) This result is not limited to post-measurement compression, but is also relevant to the measurement process itself. More specifically, for signals that can be represented by R non-zero coefficients in some native space of dimension N, the CS theory predicts that the number of measurements required is only M = Rlog(N) in contrast with Nyquist who predicts M=2N.(4) It is worth noting that a central requirement of this theory is that the measurement/sampling functions are incoherent to the space in which the signal is sparse. This requirement yields the rather surprising result that random sampling kernels/projections can be an effective measurement tool.(6) The power of random projections is one of the most significant outcomes of the recent CS revolution. Another very significant outcome is the large class of nonlinear reconstruction algorithm that enable the insertion of various additional types of prior knowledge (i.e., beyond simple sparsity) in order to improve image quality.(8-11) It is the power of these nonlinear algorithms that enables the solution to an underdetermined reconstruction problem via exploitation of priors. Our primary focus in this project as

described below, is the use of a very strong dictionary prior combined with modern nonlinear reconstruction techniques.

3.0 METHODS, ASSUMPTIONS, AND PROCEDURES

3.1 Physical system models

The DH systems shown in Figure 1 are simplified schematic representations of two candidate designs that we have studied.

Consider the full aperture (FA) image plane architecture of Figure 1a as an example.

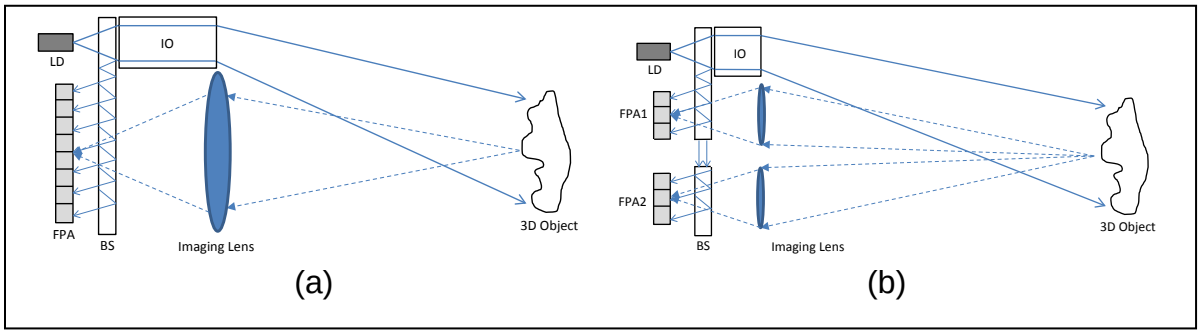

Figure 1: Various Optical Architectures for DH. (a) The Full Aperture (FA) Image Plane Architecture in which the Laser Diode (LD) Provides Coherent Illumination to an Object via Some Illumination Optics (IO). A Small Amount of Light from the LD is Picked-Off by a Beam-Splitter (BS) to Form a Reference Field. The Scattered Object Field is Imaged Using a Lens and Interferes with the Reference Field on the Focal Plane Array (FPA). (b) The Sparse Aperture (SA) Image Plane Architecture in Which the System of Figure 1a is Constructed by Tiling a Collection of Smaller Such Systems and Employing a Common Reference Beam

The DH imaging operation depicted in this Figure can be mathematically represented in a way that facilitates the application of a CS approach. Let the object be illuminated by a mono-chromatic plane wave with unit field amplitude. The scattered field leaving the object therefore, may be written as

$$O'(x,y)\exp(ikz) \text{ where } k = 2\pi/\lambda \tag{1}$$

z is the axial direction of propagation, and O'(x,y) is the complex-valued reflectance function of the object. The use of a lens in figure 1a allows us to write the object field at the focal plane (z=0) as simply

$$O(x,y) = O'(x,y)*P(x,y) \tag{2}$$

where P(x,y) is the point spread function (PSF) of the imaging system which for notational simplicity we will assume also captures the radiometric collection efficiency of the optics. In order to apply the CS formalism we will discretize the functions in this

equation according to Nyquist sampling, unwrap all 2D signals into 1D vector representations, and rewrite equation as

$$o = Po' \tag{3}$$

where o' is a N-element complex-valued vector representing the light scattered from the object, P is the linear Toeplitz operator representing convolution by the system PSF, and o is the N-element vector representing the object field incident on the FPA. Note that because this is a DH system, the FPA does not measure o directly, but rather measures a sampled version of $|o+r|^2$, where r is the N-element vector representing the reference field which is mixed with o on the FPA. The FPA output y therefore is simply the result of applying the sampling operator S to the interference signal $|o+r|^2$ so that

$$y = SD(oo^{\dagger} + rr^{\dagger} + ro^{\dagger} + or^{\dagger}) \tag{4}$$

where D indicates an operator which selects the diagonal elements of the matrix argument and the superscript † indicates Hermitian conjugate. Note that the vector outer products in this equation generate NxN matrices which after passing through the operator D produce N-element complex-valued vectors. The sampling operator for a typical FPA involves spatially integrating over disjoint local subsets of these elements to produce the M-element vector y. Alternate sampling operators may also be considered (e.g., random down-sampling or block-wise contiguous down sampling) in order to model other physically meaningful FPA measurement strategies and geometries.

3.2 Application space

There are a wide variety of defense applications for which DH may offer substantial operational benefits including surveillance, tracking, biometrics, change detection, package inspection, metrology, etc. For the purposes of this project we will focus on a notional application based on the inspection of printed circuit boards (PCBs). This application will facilitate the discussion of optical architectures and the use of relevant numerical values, making it possible to quantify the benefits of the marriage of DH and CS. It is important to note that the work described here is not limited in its applicability to PCB inspection and the PCB application is used only as a surrogate for other potential DoD applications. Like the objects found in those other potential applications, it is apparent that the objects of interest to PCB inspection may be characterized by additional constraints beyond simple sparsity. The tendency to see parallel arrays of long traces can be represented by an additional correlation structure term (e.g., mathematically characterized for example using an annulus in 2D Fourier space – a form of spectral sparsity) which serves to better condition the reconstruction problem. This improved mathematical conditioning has the effect of increasing reconstructed image quality as M (i.e., the number of measurements) and/or measurement SNR is decreased. Additional prior knowledge that has been incorporated toward this same goal includes the binary-valued nature of both the reflectance and surface relief functions (i.e., metal traces versus ceramic substrate

versus polymer resist) as well as the discrete nature of the allowed trace orientations.

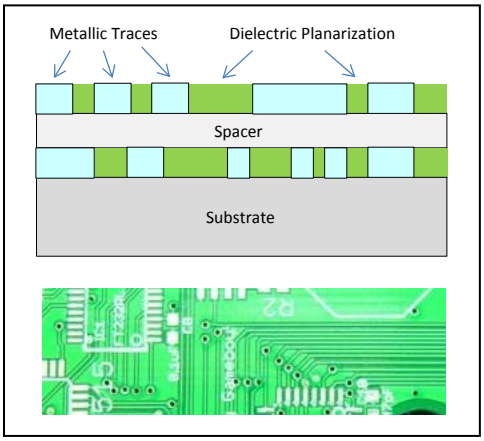

Figure 2: Modern Example Depicting Representative Characteristics of High Density Multi-Layer PCB

4.0 RESULTS AND DISCUSSION

Our project was structured into five tasks. Results will be organized and presented below according to this structure.

4.1 Task 1 - Develop linearized and/or nearly-linear DH system models suitable for use within the CS framework

Early work on Task 1 generated two operational DH models. Model 1 is a one-dimensional physics-based model based on phase shifting digital in-line holography. Limiting this initial model to 1D results in lower computational costs and will allow us to explore a larger space of physical parameters. The current physics-based model includes the following components: (a) surface relief object model, (b) diffraction-limited lens model, and (c) focal plane model. The various model parameters may be programmed as desired and we have explored a wide range of values. Mode 2 is a dictionary based compressive sensing (CS) model of the form

$$y = SPGx + n \tag{5}$$

where x is a sparse vector that generates the object via application of the dictionary G, P is the optical channel matrix, S is the FPA sampling operator, and n is the signal dependent shot noise. Because x is sparse, the product Gx produces an object with relatively few surface relief features (e.g., metal traces) on a uniform dielectric substrate. The amplitude and phase of these features are captured in the dictionary G. It is important to note that Model 2 is completely linear and therefore amenable to the wide range of CS reconstruction algorithms that have been recently published. Later work in this task was devoted to refining and exercising our physics-based model of phase shifting digital in-line holography. The various model parameters have been set

to the nominal values of wavelength = 1.1 μm, object standoff = 1m, object size = 2cm, object feature size 10μm, object feature height = 3μm, lens aperture = 22cm, lens focal length = 41cm, system magnification = 0.69, and a range of FPA pixel sizes and illumination powers. Note that for this set of parameters the diffraction-limited spot size full-width is 4.6μm and the image of a single object feature has a width of 6.9μm in the focal plane. In Figure 3 below we show the reconstructed and original object amplitude (left) and phase (right) for the case of 1μW illumination at the object, 10ms detector integration time, and 1μm detector sampling. Recall that the objects used in this work are sparse surface relief objects intended to represent printed circuit boards. For these examples we have selected a metal reflectivity of 1.0 and a dielectric reflectivity of 0.8 with a metal thickness of 3μm. Objects are created randomly with a spatial feature density of 0.01.

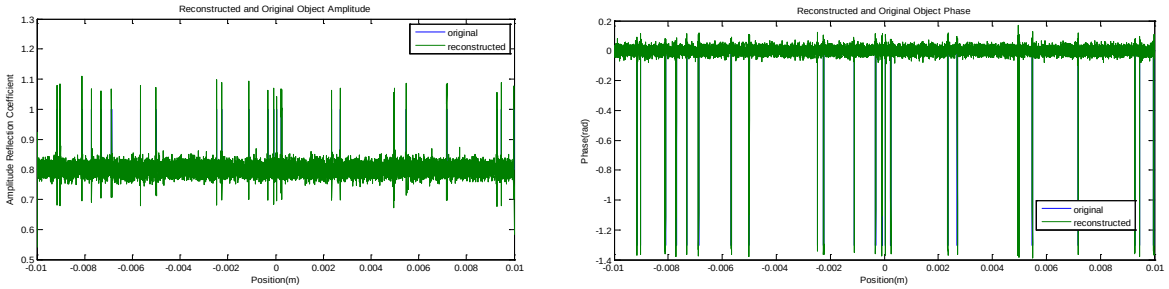

Figure 3: Original (Blue) and Reconstructed (Green) Image Plane Electric Field Using a Traditional 4-Exposure Phase Shifting Digital Holography Algorithm

In Figure 4 below, we provide an expanded view of the amplitude reconstruction using several values of focal plane sampling. All other parameters remain the same as Figure 3. We notice from this data that the 1μm detector pitch is sufficient to yield a high-quality reconstruction, albeit with the expected ringing that typically characterizes DH reconstructions. The reconstructions using 2μm and 4μm detector pixels however, show significant degradation.

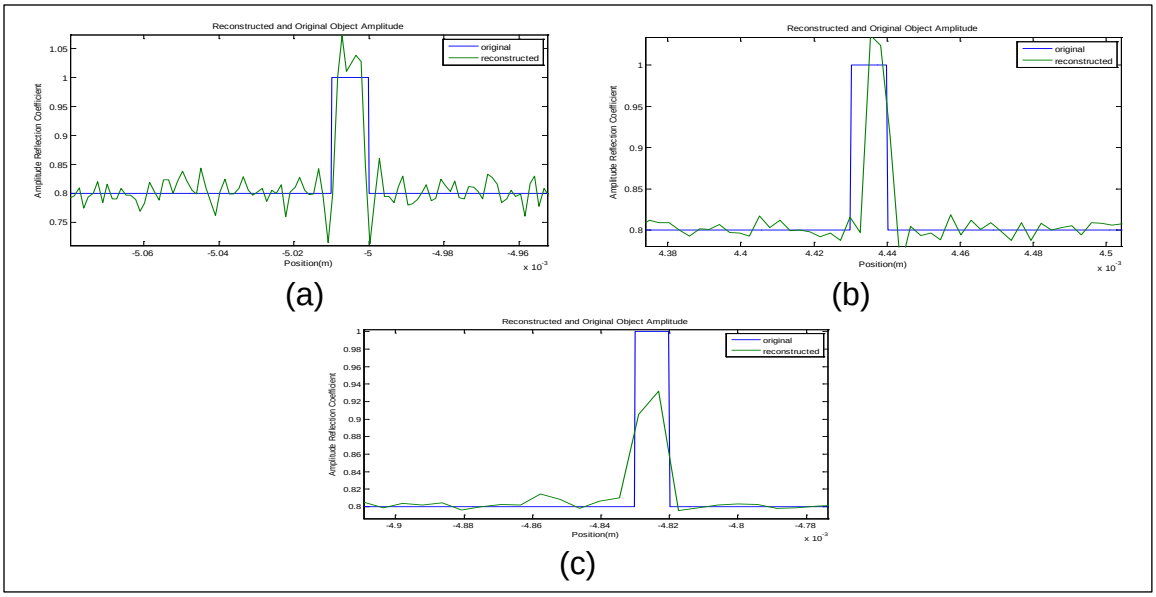

Figure 4: Zoom-In on the Amplitude of a Single Object Reflectance Feature for Three Different Values of Focal Plane Sampling (a) 1μm, (b) 2μm, and (c) 4μm

4.2 Task 2 - Develop and/or adapt CS reconstruction algorithms for use with linearized and/or nearly-linear DH measurement models

Early work in Task 2 implemented both a traditional physics-based reconstruction algorithm (i.e., backpropagation) and a corresponding CS-based post-processing algorithm. The traditional reconstruction algorithm is based on a four-exposure sequence in which four different reference phase values are used. In the absence of noise this approach completely removes the DC and ghost image terms from the in-line recording geometry. In the presence of noise and other imperfections however, this reconstruction will suffer from error. This traditional reconstruction serves as the input to our CS-based reconstruction algorithm which is based on the dictionary-sparse model described above. Our CS-based reconstruction employs the iterative soft thresholding (IST) method to find the sparse vector x (i.e., and associated reconstructed object Gx) which best matches the object estimate obtained from the traditional reconstruction algorithm. Early results showed that substantial error reduction could be obtained via this post-processing. Results from this task used the optical resolution, detector plane sampling, and reconstructed SNR outcomes from Task 1 in order to exercise our Task 2 algorithm. Some results are shown in Figure 5 below. The data in this figure is obtained by using the results from Figure 4 to estimate the effective PSF (i.e., we use a 5μm full-width sinc() for the P matrix), under-sampling factor (i.e., we used the 4μm pixel spacing to define the S matrix), and noise strength. Figure 5a is the result obtained over a small 1mm section of the reconstruction using a traditional DH holography algorithm. Figure 5b shows the result from our dictionary-based CS reconstruction method compared with the correct surface relief pattern. We see that substantial denoising and resolution improvement are obtained. Note that the algorithm is not limited to binary-valued surface relief profiles and accurately extracts all of the amplitudes in this example. This result demonstrates the expected benefit of CS to tolerate 50% fill-factor. Carefully

quantifying the degree of benefit and its dependence on system parameters such as object standoff, laser power, and NEP is the subject of Task 4.

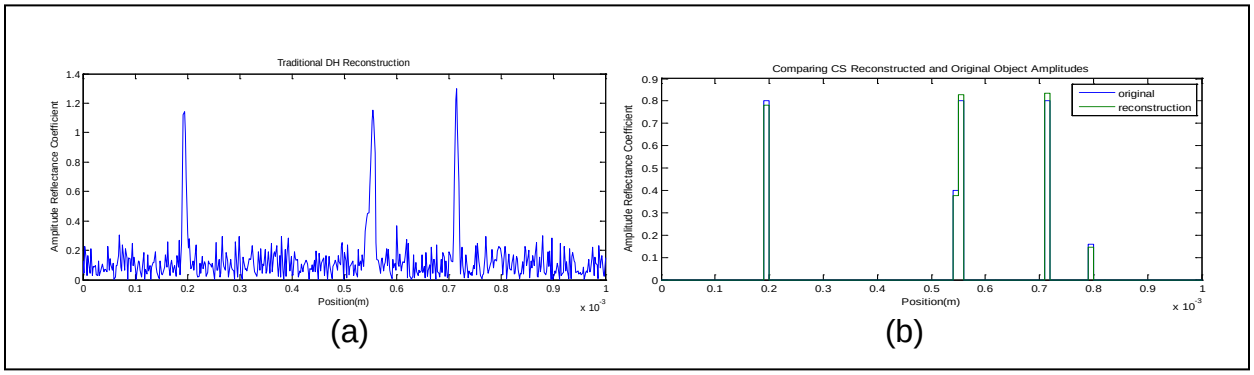

Figure 5: Traditional (a) and CS-Inspired Reconstruction of a 1mm Portion of a Non-Binary Surface Relief Object. Optical Resolution, Noise, and Under-Sampling are Comparable to Figure 4c

4.3 Task 3 - Investigate additional signal and task priors to further improve the quality of DH reconstructions

Extending the 1D models described above into two-dimensions was a primary outcome of this task. In the process of building these improved 2D models we were able to also include (a) optical performance informed by the five primary Seidel aberrations (i.e., in additional to the earlier diffraction-limited performance), (b) the binary-valued nature of the PCB amplitude and phase functions, and (c) spatial correlation between the amplitude and phase reconstructions. Figure 6 below shows some preliminary results from the 2D model. Figure 6a below depicts the original sparse object with dictionary sparsity level = 18. Because this is a surface relief object, only the amplitude is shown. The phase function is identical. Figures 6b and 6c below presents the amplitude and phase reconstructions obtained using a traditional backpropagation algorithm when the measurement is obtained without under-sampling. We can see from this data that the traditional algorithm works very well at these SNR levels in the absence of under-sampling. All other system parameters are as described above (i.e., wavelength = 1.1 μm, object standoff = 1m, object size = 2cm, object feature size 10μm, object feature height = 3μm, lens aperture = 22cm, lens focal length = 41cm, system magnification = 0.69, 1μW illumination at the object, and 10ms detector integration time). Figure 6d and 6e is for 4x under-sampling. We see that the conventional reconstruction algorithm completely fails at these modest degree of under-sampling and noise levels. This may be contrasted with the data shown in Figure 7 below, where we have repeated the simulation experiment of Figure 6 using our CS reconstruction algorithm. This results demonstrates that our nonlinear CS algorithm is capable of producing near-perfect reconstructions at 4x under-sampling and still-useful reconstructions even with 16x under-sampling. Note that the results shown in Figure 6 and 7 are based on the FA architecture.

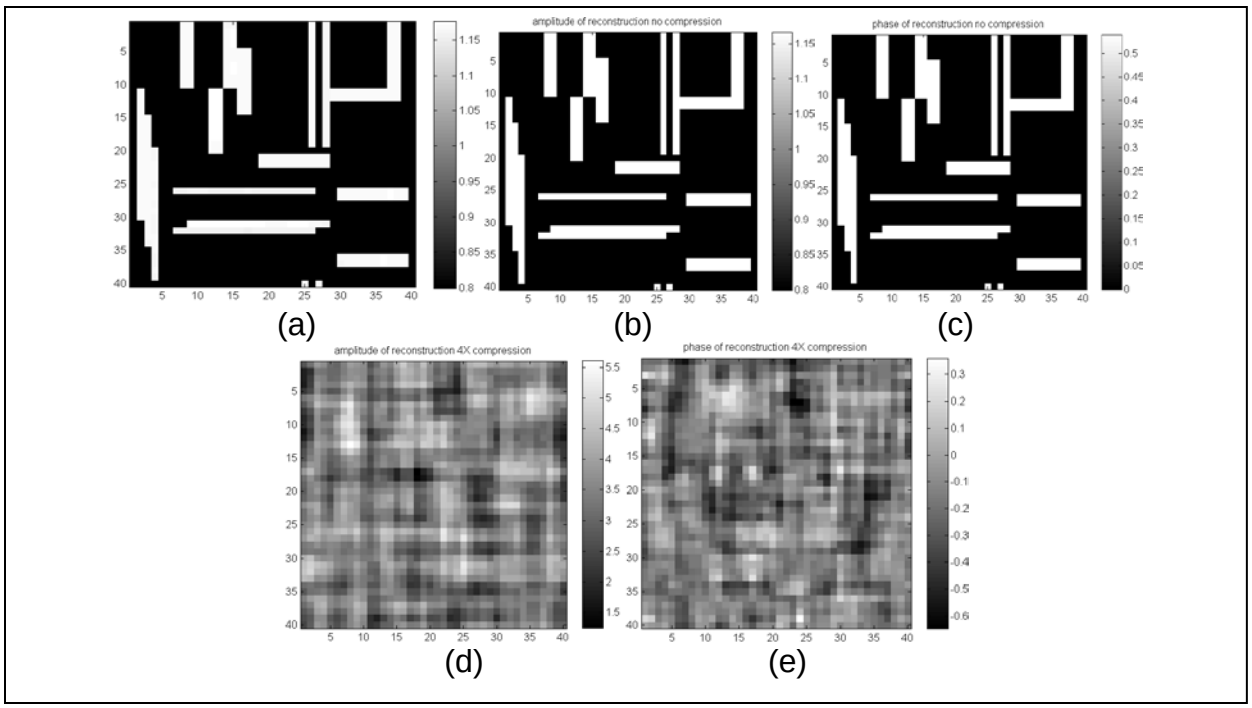

Figure 6: Extension of 1D results into 2D. (a) Sparse Object Amplitude (Phase is Identical for Surface Relief Pattern), Reconstructions of (b) Amplitude and (c) Phase Using a Conventional Backpropagation Algorithm without Under-Sampling (d) and (e) are Amplitude and Phase Results Obtained from 4x Under-Sampling

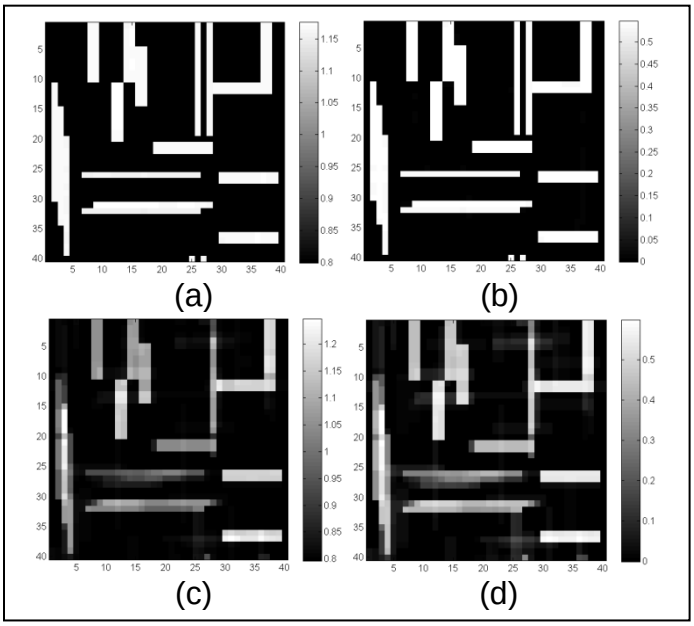

Figure 7: CS Reconstruction of the Object Shown in Figure 6a and Under the Same Measurement Conditions. (a) Amplitude and (b) Phase Reconstruction for 4x Under-Sampling. (c) and (d) Correspond to 16x Under-Sampling

4.4 Task 4 - System study for full-aperture DH system

In this task, we undertook a systematic study of reconstruction performance for the FA architecture. The system layout and associated numerical parameters (i.e., slightly different from those reported above) are shown in Figure 8 below. The variables that we studied/varied were (a) exposure time (i.e., which together with the illumination power determines the shot noise level), (b) object sparsity, and (c) degree of under-sampling in the FPA. We found the expected trends in all of these variables. For example, increasing exposure time from 10ms to 100ms was found to reduce reconstruction error. Increasing the number of sparse coefficients required to describe the object from 11 to 18 (i.e., making the object less sparse) was found to increase reconstruction error. And the most severe influence on reconstruction quality was due to the degree of under-sampling, with 16x under-sampling yielding reconstruction quality far inferior to the nearly-perfect reconstructions obtained at only 4x under-sampling. Some representative data is shown in Figure 9 below. We notice from this data that 16x under-sampling with sparsity=11 yields nearly identical performance to 8x under-sampling with sparsity = 18. Representative reconstructed images are shown in Figure 10 below and demonstrate that this level of RMSE < 0.1 corresponds to essentially perfect reconstruction.

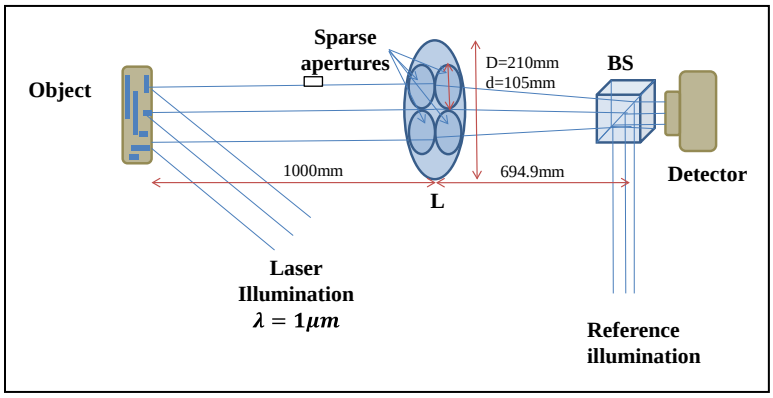

Figure 8: Physical System Layout Used in Task 4 and Task 5 Studies. BS: Beam Splitters, L: Lens (210mm Diameter, 410mm Focal Length), M: Mirror, Object is @ 1000mm from the Lens, Object Feature Size: 2.436μm, Detector Pixel Size 2.436μm, Illumination Beam Angle 10^0

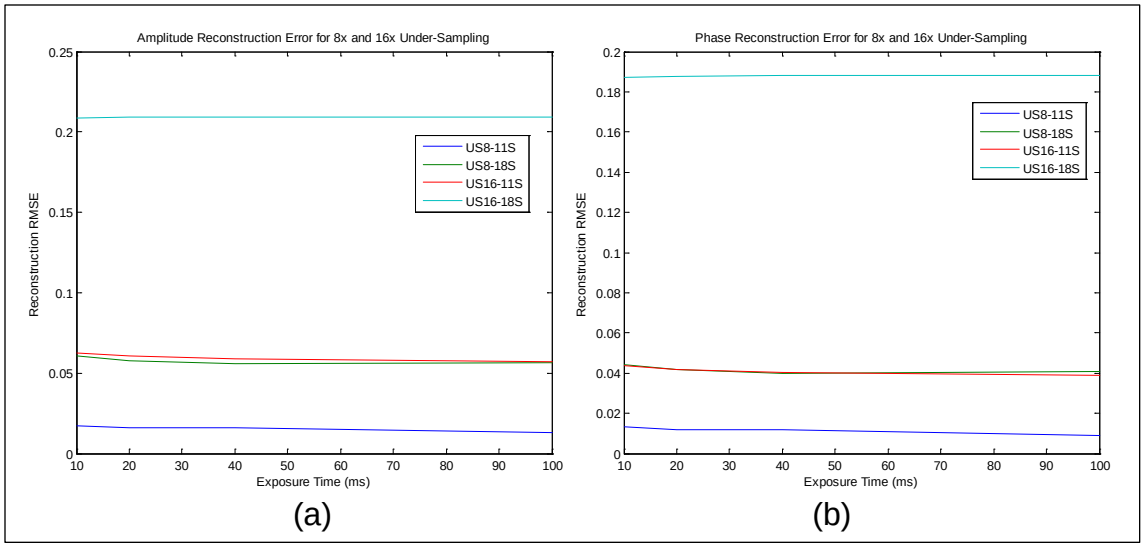

Figure 9: Reconstruction RMSE Versus Exposure Time Using the FA System for (a) Amplitude and (b) Phase Reconstructions with 8x and 16x Under-Sampling (US) and Object Sparsity (S) Levels of 11 and 18

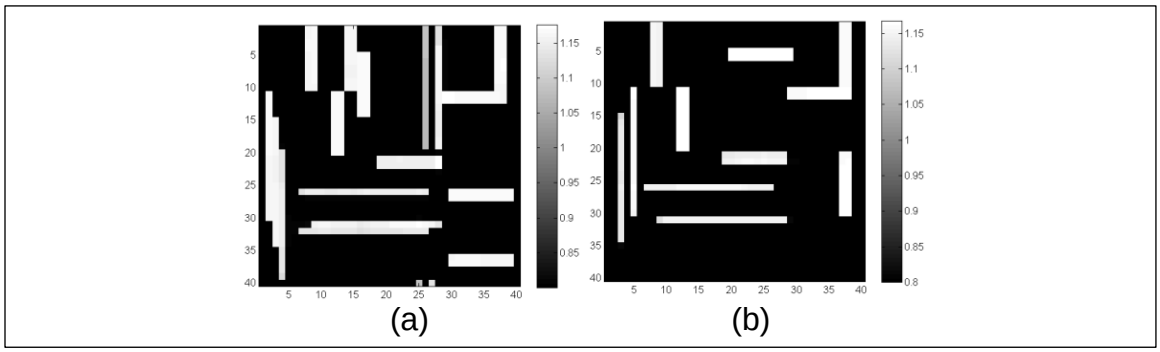

Figure 10: Example Reconstructions Corresponding to Approximately RMSE = 0.05. (a) 8x Under-Sampling with Sparsity = 18 and (b) 16x Under-Sampling with Sparsity = 11

4.5 Task 5 - System study for sparse aperture DH system

A significant benefit of holographic measurement is the ability to synthesize large coherent apertures from a collection of small sparse apertures. In this task we undertook a systematic study of sparse aperture digital holography aided by CS inspired reconstruction algorithms. Because it is important to understand how coherent aperture synthesis impacts reconstructed image quality, we have studied both single aperture (i.e., using only one of the small lenses depicted in Figure 8) and dual-aperture (i.e., using a diagonal pair of small lenses) approaches. Figure 11 presents some representative results from this study. Note that the RMSE obtained using a single small aperture (i.e., shown in Figure 11a) is quite poor for all values of exposure time, under-sampling, and sparsity. This is because the object feature size is well-below the diffraction-limited resolution of a single small aperture. From Figure 11b we see that the synthetic aperture is able to recover this lost resolution and provide excellent RMSE. Also notable is the stronger dependence on exposure time (i.e., compared with Figure 9) which arises from poorer light collection efficiency of the sparse aperture system.

Figure 12 presents example reconstructions from the 16x under-sampled case with sparsity = 18. Note that the reconstruction using a single aperture (Figure 12a) is very poor while the result using the synthesized aperture (Figure 12b) is excellent.

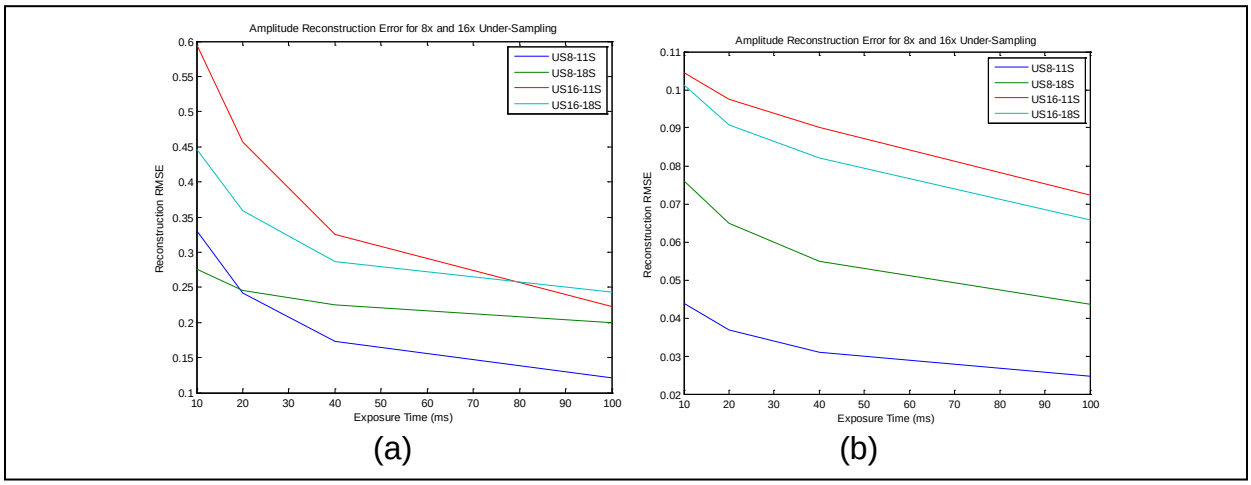

Figure 11: Amplitude Reconstruction RMSE Versus Exposure Time Using (a) a Single Small Aperture and (b) a Diagonal Pair of Small Apertures with 8x and 16x Under-Sampling (US) and Object Sparsity (S) Levels of 11 and 18

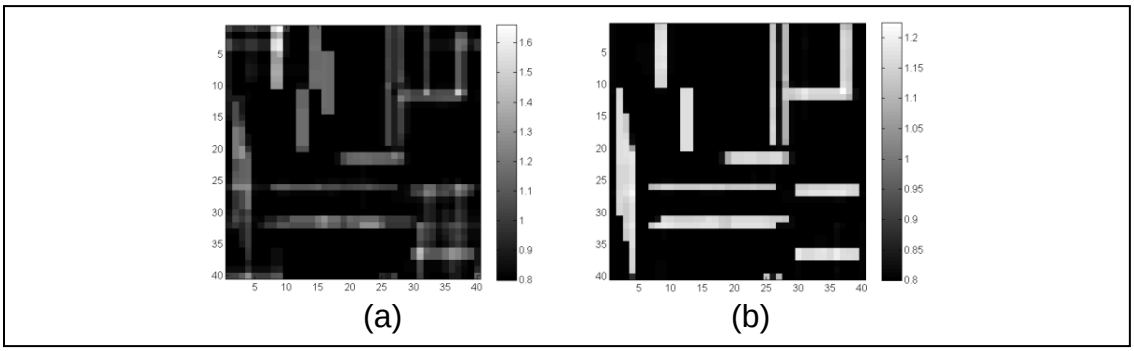

Figure 12: Amplitude Reconstructions from a Sparse Aperture System Using 16x Under-Sampling and Object Sparsity = 18. (a) Reconstruction Obtained from a Single Small Aperture and (b) Reconstruction Obtained from a Diagonal Pair of Small Apertures

5.0 CONCLUSION

This report has described a new approach to the reconstruction of digital holographic images. We have developed a nonlinear reconstruction algorithm inspired by compressive sensing, which exploits a dictionary prior and yields high quality amplitude and phase images from severely under-sampled measurements. We show that although traditional backpropagation reconstruction methods fail at 4x FPA under-sampling, our new algorithms can successfully reconstruct essentially perfect (i.e., RMSE < 0.1) 3D images from 16x under-sampled data. We demonstrate that the dependence on SNR is quite weak for the full aperture system operating at reasonable standoff, illumination power, and collection aperture. We also demonstrate that these same CS-inspired reconstruction algorithms can be used to achieve excellent synthetic

aperture performance (i.e., clearly demonstrating full-aperture resolution recovery) from sparse collection lenses.

5.1 Milestone Review

Milestone 1: Completion of DH models suitable for use within CS framework
This milestone has been met by the forward model results presented in Task 1 and the nonlinear reconstruction algorithm described in Tasks 2 and 3. The forward models include all relevant physical effects such as illumination power, exposure time, FPA sampling, optical aberrations, etc. The reconstruction algorithms leverage a dictionary prior and a nonlinear iterative soft thresholding technique to achieve high quality reconstructions that satisfy both the measurement and sparsity constraints.

Milestone 2: Demonstration of CS reconstruction achieving 50% DH fill factor

Milestone 3: Demonstration of CS reconstruction achieving 25% DH fill factor
These milestones were intended to represent increasing algorithm complexity over the life of the project. Early in the project we were able to achieve reconstructions at 2x under-sampling (i.e., 50% fill-factor) as depicted in Figure 4. By the end of our project we were regularly reconstructing near-perfect 3D images (i.e., amplitude and phase) from 16x under-sampled measurements (i.e., 12.5% fill-factor), easily satisfying both milestones 2 and 3.

Milestone 4: Graphical results that quantify reconstructed full-aperture DH image quality versus various physical parameters.
Section 4.4 Task 4 presents example graphical results for the full-aperture system study.

Milestone 5: Graphical results that quantify reconstructed sparse-aperture DH image quality versus various physical parameters.
Section 4.5 Task 5 presents example graphical results for the sparse-aperture system study.

6.0 REFERENCES

1. E. T. Whittaker, “On the functions which are represented by the expansions of the interpolation theory,” Proc. Royal Soc. Edinburgh, Sec. A, 35, pp. 181-194, 1915.
2. H. Nyquist, “Certain topics in telegraph transmission theory,” Trans. AIEE, 47, pp. 617-644, 1928.
3. D. Taubman and M. Marcellin, JPEG2000: Image Compression Fundamentals, Standards and Practice, (Kluwer Academic Publisher, 2001).
4. Y. Tsaig and D. Donoho, “Compressed sensing,” IEEE Trans. Information Theory, 52, pp. 1289-1306, 2006.
5. D. Donoho and Y. Tsaig, “Extensions of compressed sensing,” Signal Processing, 86(3), pp. 533-548, 2006.
6. E. Candes and J. Romberg, “Signal recovery from random projections,” Proc. SPIE 5674, 76, 2005.
7. E. Candes and T. Tao, “Near-optimal signal recovery from random projections: Universal encoding strategies?” IEEE Trans. Information Theory, 52, pp. 5406-5424, 2006.
8. E. Candes and T. Tao, “Decoding by linear programming,” IEEE Trans. Information Theory, vol.51, no.12, pp. 4203- 4215, Dec. 2005.
9. J.A. Tropp, A.C. Gilbert, “Signal recovery from random measurements via orthogonal matching pursuit,” Information Theory, IEEE Transactions, Volume 53, No. 12, pp. 4655 – 4666, 2007.
10. Yonina C. Eldar and Moshe Mishali. “Robust recovery of signals from a structured union of subspaces,” IEEE Trans. Information Theory, vol. 55, no. 11, pp. 5302-5316, 2009.
11. H. Rauhut, K. Schnass and P. Vandergheynst, “Compressed sensing and redundant dictionaries,” IEEE Trans. Information Theory, vol. 54, no. 5, pp. 2210-2219, 2008.

List of Symbols, Abbreviations, and Acronyms

Symbol/Acronym/ Abbreviation	Description
BS	Beam-Splitter
CS	Compressive Sensing
DH	Digital Holography
DoD	Department of Defense
FA	Full Aperture
FPA	Focal Plane Array
IO	Illumination Optics
LD	Laser Diode
PCB	Printed Circuit Boards
PSF	Point Spread Function
RMSE	Root Mean Squared Error
SA	Sparse Aperture
SNR	Signal to Noise Ratio
NEP	Noise Equivalent Power
IST	Iterative Soft Thresholding